Abrupt Changes in the Timing and Magnitude of the North Atlantic Bloom Over the 21st Century

Stephen Kelly[1] , Ekaterina Popova[1] , Andrew Yool[1] , Fatma Jebri[1] , Sophy Oliver[1] , and Meric Srokosz[1]

[1]National Oceanography Centre, Southampton, UK

Abstract The North Atlantic subpolar gyre (SPG) is a key region for the North Atlantic bloom (NAB), the phytoplankton foundation of the regional food web. The NAB depends on nutrients seasonally introduced into the surface ocean by deep winter convection. Under climate change, this pattern is threatened by increasing water column stratification, representing a potential "tipping point" in the Earth system, and may "collapse" as a result. We investigate changes in winter mixing and the impacts on the SPG and the northern North Atlantic using a spread of future projections from a low-resolution Earth system model (UKESM) and a high-warming projection of a high-resolution ocean-only configuration of the same model (NEMO-MEDUSA). Both models project significant declines in the strength of the NAB during the 21st century. In UKESM, this occurs across all projections, but with low spatiotemporal coherence. In NEMO-MEDUSA, changes in mixed layer depth, nutrients, and chlorophyll concentrations are abrupt and more highly spatiotemporally correlated. We find a >30-day phenological shift in the peak of the bloom aligned with the timing of this change, which may affect food web dynamics. Defining "collapse" as halving of surface chlorophyll, we find that the NAB collapses this century regardless of future projection. However, the spatial-temporal coherence of the timing and abruptness of this collapse is greater in our high-resolution model. Because key physical processes driving biogeochemical responses are poorly represented in low-resolution models, especially at high latitudes, this suggests that higher resolution may be essential for predicting abrupt and irreversible changes, particularly those involving ecosystem dynamics.

Plain Language Summary The North Atlantic bloom, or NAB, is the annual increase in microscopic algae that occurs across the region every spring. It is dependent on nutrients brought to the surface by deep winter mixing, and it is particularly ecologically important because it provides the base of food chains in the North Atlantic. However, a warming climate may change both the magnitude and spatial pattern of deep-ocean mixing, reducing nutrient supply to the surface and diminishing the NAB. It has been suggested that these changes could occur abruptly if the climate system crosses a critical "tipping point" of warming. Here, we use a low-resolution Earth system model (ESM) and a high-resolution ocean model to simulate the future of the NAB. Our projections find that the NAB declines, with abrupt changes occurring from the year 2040. The bloom is also projected to occur earlier in the year, which may affect the wider food web. We also find the high-resolution model presents highly coherent spatial and temporal change, with the lower resolution ESM potentially offering more limited skill in predicting abrupt and irreversible changes in the marine systems.

1. Introduction

The concept of climate tipping elements was introduced in Walker (2006) and further expanded upon in Lenton et al. (2008) to describe large-scale features of the Earth system that are projected to undergo non-linear, abrupt changes to an objectively different state if a critical threshold (or "tipping point") of climate change is exceeded. Significantly, such nonlinear changes could be irreversible over human timescales (decadal to centennial or beyond), and anthropogenic warming is predicted to trigger several climate tipping points. Various potential tipping elements have been identified in the climate system, including polar ice sheets, coral reefs, and the North Atlantic subpolar gyre (hereafter SPG), as having so-called tipping points (Armstrong McKay et al., 2022).

The SPG is a dominant large-scale cyclonic ocean gyre in the North Atlantic between 45°N and 65°N, driven by wind and heat uptake (Bersch et al., 2007; Biri & Klein, 2019; Häkkinen & Rhines, 2004). The upper branch of the Atlantic Meridional Overturning Circulation (AMOC) brings up warm salty waters via the Gulf Stream, North Atlantic Current, and Irminger Current, where decreased buoyancy due to heat losses leads to deep convection in

Visualization: Stephen Kelly, Andrew Yool
Writing – original draft: Stephen Kelly, Ekaterina Popova, Andrew Yool, Sophy Oliver
Writing – review & editing: Stephen Kelly, Ekaterina Popova, Andrew Yool, Fatma Jebri, Sophy Oliver, Meric Srokosz

the SPG; this occurs in the Labrador and Irminger Seas. The deep water formed here during wintertime densification is the main contributor to the lower limb of the AMOC (Reverdin et al., 2019; Rhein et al., 2011; Sanchez-Franks et al., 2024; Yashayaev & Loder, 2017) and is the most important site of anthropogenic carbon dioxide storage (Daniault et al., 2016; Khatiwala et al., 2013; Pérez et al., 2010, 2013). Formal definitions of the SPG based on oceanographic conditions exist (e.g., Foukal and Lozier, 2017), but here, we focus on geographically bounded regions.

Due to increasing water column stratification and stability, ultimately driven by climate change, the North Atlantic SPG may be on the verge of a tipping point characterized by a deep convection "collapse" (Armstrong McKay et al., 2022). The SPG is believed to be bistable, characterized by a strong mode in which saline subtropical waters are advected to the gyre's center, causing strong convection, and a weak mode in which this is inhibited (Born et al., 2013; Sgubin et al., 2017); here, "collapse" refers to a shift from the strong to the weak mode of the SPG. Impacts could unfold on a decadal timescale (Swingedouw et al., 2021), potentially leading to a regional cooling of ~2 to 3°C and a suppression of global warming by up to ~0.5°C (Sgubin et al., 2017; Swingedouw et al., 2021); a northward-shifted jet stream, increased seasonality, and intensified weather extremes in Europe (Armstrong McKay et al., 2022; Sgubin et al., 2017; Swingedouw et al., 2021); sea level rise on the northeast seaboard of North America, a southward shift of the intertropical convergence zone, risking collapse of the West African monsoon, and affecting the South American monsoon (Armstrong McKay et al., 2022; Bozbiyik et al., 2011).

The impacts of North Atlantic SPG collapse on marine ecosystems represent a critical knowledge gap. These ecosystems are ultimately supported by the North Atlantic bloom (NAB), the seasonal surge in phytoplankton biomass that occurs each spring, and provides the base of the regional food web (Melle et al., 2014). Specifically, deep winter convection in the northern North Atlantic, most notably in the SPG region, is followed by spring restratification, creating growing conditions that are conducive to a significant spring phytoplankton bloom, of global-scale importance (Martin et al., 2011). However, this phenomenon is likely to diminish if the strength of seasonal convection—and deep nutrient replenishment—decreases, with consequences for marine resources such as fisheries (e.g., Jacobsen et al., 2022) and the wider ecosystem (e.g., Beaugrand et al., 2003). Alongside the magnitude of potential changes to the NAB, climate change may also initiate changes in the phenology (the relationship between climate and seasonal ecological cycles; Asch, 2019) of the bloom and species, which depend on it either directly or at higher trophic levels (Cole et al., 2012). An earlier spring bloom can lead to earlier peaks in egg production for copepods, which feed directly on the NAB, in turn possibly leading to earlier Atlantic cod spawning (McQueen & Marshall, 2017). However, the copepods (and higher trophic levels) have synchronized their interactions over evolutionary timescales (Friedland et al., 2016; Payton et al., 2022) and therefore cannot adapt to a changed bloom timing instantaneously, leading to a widening "seasonal mismatch" between fish spawning and peak plankton biomass with climate change (Edwards & Richardson, 2004; Ferreira et al., 2021; Häfker et al., 2023). These factors underscore the necessity of understanding how the SPG and the NAB will change in the coming century.

Previous research into the future of the high-latitude North Atlantic predicts that the region will experience increased stratification (Kwiatkowski et al., 2020; Sgubin et al., 2017) and a decrease in surface nutrients (Lavoie et al., 2017; Sein et al., 2015), leading to a decrease in net primary production and export production (Fu et al., 2016; Kwiatkowski et al., 2020; Nakamura & Oka, 2019; Yool et al., 2015). Furthermore, model experiments have explored potential changes in the timing of the bloom; changes in the phenology of the bloom may be detectable sooner than changes in its magnitude (Sparks & Menzel, 2002). Studies in the northern North Atlantic suggest that an earlier onset and/or peak of the NAB is likely by the end of the century, with blooms occurring earlier in the year at a rate of approximately 5 days per decade in high latitudes (Henson et al., 2018).

Hieronymus et al. (2024) used two CMIP6 models under a high-emissions scenario to investigate abrupt changes in net primary production in the North Atlantic and projected that spatiotemporally correlated changes would occur in the future seasonal cycle of mixed layer depth. Under the scenarios they investigated, abrupt changes were projected to occur within the first half of this century; this demonstrates that shifts in NAB phenology are an issue of pressing importance, and the authors identified further research with more models and scenarios as a priority.

Here, we investigate a regime change in the NAB using both an ensemble of projections for a range of Shared Socioeconomic Pathways (SSPs) from a low-resolution Earth system model (ESM) and a high-resolution forced-ocean model. We aim to answer three main questions: (1) Will the NAB collapse in the coming decades and, if so, when? (2) Will the changes be gradual or abrupt? (3) How will the phenology of the NAB change?

2. Methods

The methodology section is structured as follows. First, Section 2.1 provides an overview of descriptions of the UKESM (UK Earth System Model) and high-resolution NEMO (Nucleus for European Modeling of the Ocean) models, as well as the future projection simulations used here. Next, Section 2.2 describes the observational data sets used for model validation. Finally, Section 2.3 describes the analysis methodologies used, including for region selection, changepoint analysis, and phenology.

2.1. Models

For the work here, simulations using two related models are used: UKESM, a fully coupled Earth system model (Yool et al., 2021); and NEMO-MEDUSA, a high-resolution ocean-only model projection (Yool et al., 2013). The latter model is the main focus of this study, but this is framed—and forced by—the UKESM model.

2.1.1. UKESM1

UKESM1 takes its physical core (atmosphere, ocean, and land) from the climate model, HadGEM3-GC3.1 (Kuhlbrodt et al., 2018; Williams et al., 2018). Earth system process additions to this include terrestrial carbon and nitrogen cycles that include dynamic vegetation and land-use change (Clark et al., 2011; Wiltshire et al., 2021); a unified troposphere-stratosphere chemistry model that is coupled to a multispecies aerosol scheme (Archibald et al., 2020; Mulcahy et al., 2018); and marine biogeochemistry including nitrogen, silicon, iron, carbon, and oxygen cycles and the exchanges of climatically active dimethyl sulfate (DMS) and primary marine organic aerosols (PMOA). UKESM1's ocean component is composed of the NEMO v3.6 ocean physics model, the CICE v5.1.2 sea-ice model, and the MEDUSA v2.1 marine biogeochemistry model (Storkey et al., 2018; Yool et al., 2021). Relevant Earth system couplings for the ocean component are the ocean carbon cycle's coupling to atmospheric CO_2 concentrations (and climate), the ocean's iron cycle coupling to dust deposition (ultimately derived from bare soil in the land component), and ocean-aerosol coupling of DMS and PMOA emissions. Sellar et al. (2019) provide a summary overview of UKESM1 and its component submodels, including details about its development, tuning, and CMIP6 simulations. Yool et al. (2021) provide additional details on UKESM1's ocean component, and specifically evaluate this, both physically and biogeochemically.

The simulations of UKESM1 used here cover the historical (1850–2014) and scenario (2015–2100) simulation periods. Historical period simulations are initialized using model states drawn from selected timepoints of the model's preindustrial control (see Sellar et al., 2019; Yool et al., 2020). Following the completion of the historical period, a range of extensions to the end of the 21st century were performed. These utilized five different scenarios of anthropogenic carbon emissions, land-use change, etc., based on the Shared Socioeconomic Pathways (SSP) framework (O'Neill et al., 2016). To examine the broadest range of model behavior in the SPG, SSPs 126, 245, 370, 434, and 585 were used in the analysis shown here.

The ocean in UKESM1 uses the extended ORCA1 grid (eORCA1) with a horizontal resolution of approximately 1 degree on a tripolar grid (Madec & Imbard, 1996) and with enhanced equatorial resolution.

2.1.2. NEMO-MEDUSA

While UKESM1 represents many ocean features and dynamics well (see Yool et al., 2021), a limitation is its use of a low-resolution model domain. This impacts the realism of its representation of the circulation and water mass features that define and frame the North Atlantic SPG. To address this, here, we use an ocean-only configuration run at much greater grid resolution and forced by atmospheric boundary properties from a fully coupled UKESM1 simulation.

The model grid used here retains the same tripolar structure as in UKESM1, but has a horizontal resolution of approximately 1/12-degree. Its vetertical resolution is the same 75 depth levels as in UKESM1. Due to the passage of time, the NEMO version used here is v4.0 and incorporates a small number of technical and scientific improvements from that used in UKESM1. The MEDUSA version used is identical to that used in UKESM1. Meanwhile, the more recently developed SI3 sea-ice model (Vancoppenolle et al., 2023) replaces the CICE model used in UKESM1.

Because of the high computational cost of this high-resolution NEMO-MEDUSA configuration (even in ocean-only mode), only a single-future scenario run is undertaken compared to the five used here from UKESM1. As noted, this simulation is run in ocean-only mode and is forced at the surface using output from a (fully coupled) simulation of UKESM1.1 (see below). This mode takes bulk properties of the atmosphere from its lower boundary (air temperature, humidity, and wind velocities), as well as downward fluxes of heat and freshwater (including riverine inputs of freshwater), and uses these with bulk formulae to calculate ocean-atmosphere exchanges of heat, freshwater, and momentum. As the atmosphere is noninteractive in this mode, freshwater imbalances can occur (i.e., where rainfall is not balanced with evaporation at global scale). Sea surface salinity (SSS) is additionally relaxed at the surface to prevent unrealistic drift. All the fields of atmospheric quantities and SSS used here are taken from the same UKESM1.1 simulation.

The simulated period used here is 1980–2100, and the simulation was initialized in two steps. First, the year 1850 state of the UKESM1.1 simulation from which the surface forcing was taken was upscaled and used to initialize an ocean-only NEMO-MEDUSA simulation at 1/4 degree. This latter configuration entirely parallels the main 1/12-degree configuration but at a lower resolution. Second, this parallel model was simulated from 1850 to 2100, and its year 1980 state was itself upscaled and used to initialize the 1/12-degree configuration. Note that, as a result of this traceable use of existing model states, biases introduced into the long spin-up period of UKESM1 (Yool et al., 2020) are inherited by all UKESM1 simulations and the 1/12-degree simulation as well.

Regarding the choice of future scenario, and reflecting changes in expectations for realistic "high emissions" futures (e.g., Ritchie & Dowlatabadi, 2017), here, we make use of the SSP370 scenario, "Regional Rivalry" (O'Neill et al., 2016). This scenario reaches 7.0 W m^{-2} of warming by year 2100 compared to 8.5 W m^{-2} in the most extreme UKESM1 simulation (SSP585).

As noted above, rather than use one of the UKESM1 simulations, a UKESM1.1 simulation was selected to provide surface forcing and (ultimately) the initial condition for the 1/12-degree simulation. This choice was motivated by improvements to UKESM1 that removed a cold bias during historical simulations (principally by improving the representation of SO$_2$ dry deposition). This revised UKESM1 version is fully documented in Mulcahy et al. (2023).

2.2. Observational Data Sets

The following observational data sets were used for validation purposes. Validation is presented in Section S1 of the Supporting Information S1.

2.2.1. Upper Mixed Layer Depth (MLD)

An objectively analyzed climatological (2005–2017) set of monthly means for upper mixed layer depth, calculated from profiles of potential temperature and potential salinity, based on a density criterion (the depth at which seawater density exceeds the 10-m density by 0.125 kg m^{-3}), was taken from the World Ocean Atlas to validate the modeled mixed layer depth (Locarnini et al., 2019). This density threshold was chosen over a tighter threshold (e.g., the default 0.01 kg m^{-3} threshold used in NEMO) as it is well-suited to data sets averaged into monthly means (Kara et al., 2000; Treguier et al., 2023). For the figures in the validation section (S1), the model mixed layer depth is recalculated from modeled temperature and salinity based on the same density threshold as used in Locarnini et al. (2019).

2.2.2. Surface Dissolved Inorganic Nitrogen (DIN)

Objectively analyzed climatological (again 2005–2017) monthly means of inorganic nutrients were taken from World Ocean Atlas (Garcia et al., 2019). As the nitrogen cycle is the base currency of MEDUSA, DIN was chosen as the most appropriate variable to validate the model performance against.

2.2.3. Surface Chlorophyll (CHL)

Surface chlorophyll concentrations were validated against the Climate Change Initiative (CCI) v5 L4 monthly 4-km resolution data set, downloaded from Copernicus Marine Environmental Monitoring Service (CMEMS, https://marine.copernicus.eu/access-data), calculated from satellite observations of ocean color as described by Gohin et al. (2002) and updated by CMEMS following the same method since. To capture the full spring boom,

climatological (2010–2019) summers (defined to be May–September) were compared against modeled surface CHL concentrations.

2.3. Analysis

2.3.1. Selection of Geographical Regions (Boxes)

In order to explore the long-term trends in modeled MLD, DIN, and CHL over the 21st century, five geographical regions (hereafter "boxes") were chosen to sample different regimes (identified from features in Figures 3g–3l) within the northern Atlantic; the time series of annual maxima for each NAB variable are shown in Section 3.3 to give an illustrative overview of how the North Atlantic is projected to change before moving on to cell-by-cell analysis. The regions chosen are shown in Figure 4 and are as follows:

- *Labrador Sea* (57–60°N, 47–57°W): chosen to sample the western portion of the subpolar gyre where the collapse in deep winter convection was most pronounced in preliminary analysis of changes in upper mixed layer depth.
- *Irminger Sea* (58–63°N, 32–40°W): chosen to sample the eastern portion of the SPG, which preliminary analysis indicated behaved differently to the west of the SPG (Labrador box).
- *Iceland Sea* (66–69°N, 7–15°W): chosen to illustrate the changes in a region that preliminary analysis suggested would show an opposite trend to much of the northern North Atlantic; see Figure 3g where a small increase in the NAB can be seen.
- *Greenland Sea* (71–76°N, 10–20°W): chosen to sample another region of deep winter mixing in the current climate, to explore how mixing changes in the coming decades.
- *West of Scotland* (56–61°N, 8–18°W): preliminary analysis indicated that the northeast of the Atlantic Ocean could be a key region for decline of the NAB; this region was also chosen because of its importance to Western European fisheries.

2.3.2. Changepoint Analysis

A changepoint analysis function (`findchangepts`, a MATLAB subroutine) was applied to detected significant abrupt changes in time serieses of annual maxima (calculated from monthly means) for MLD, DIN, and CHL. This algorithm is based on minimizing a loss function (Killick et al., 2012) such that it minimizes the sum of residual squared errors on either side of a candidate changepoint local statistical property (e.g., mean).

This parametric method is as follows: first, the algorithm partitions the time series into two sections. It then computes the local statistical property (here, the mean) for each section, computes the sum of residual squared errors compared to said mean either for each section, and returns detected changepoints where the residual error is minimized. This changepoint detection technique is effective in distinguishing abrupt changes from trends in time serieses (Beaulieu & Killick, 2018) and showed better performance than other approaches including Rodionov (2004)'s regime shifts method and Ruggieri (2013)'s Bayesian linear regression multiple changepoint detection approach. Both the magnitude and timing of the identified changepoint are presented in the results, and the root of residual squared errors is also reported.

The function was applied to find only the most significant changepoint (if any) in each case. Changepoints detected near to either end of a time series are not necessarily reliable due to the short time before/after the candidate changepoint not being sufficient to demonstrate a truly significant change (cf. Jebri et al., 2024), and therefore candidate changepoints detected during the first or last decade of each time series were discarded from our analysis.

Prior to applying the changepoint analysis, Fourier analysis (shown in Supporting Information S1, Figure S10) was performed to identify the dominant mode of variability. The dominant mode was found to be multidecadal, demonstrating that the results would not be unduly influenced by interannual variability. The analysis was repeated with a LOESS-smoothed time series (Figure S11 in Supporting Information S1), and the results did not change appreciably.

While the identification of changepoints is completed efficiently using a combination of dynamic programming and pruning (Beaulieu & Killick, 2018), the method does not return an uncertainty estimate for the timing of the changepoint. However, a residual error for each detected changepoint is provided. This metric compares the sum of squared "errors", relative to the temporally local mean, for the periods from the beginning of the time series to

Table 1
Changepoint Analysis Metrics (Timing, Root of Squared Residual Error, Magnitude, and Abruptness) for the Time Series of Annual Maxima (2000–2100) for Upper Mixed Layer Depth, Surface Dissolved Inorganic Nitrogen, and Surface Chlorophyll for Each of the Boxes

Region		MLD	DIN	CHL
Greenland	Changepoint year	N/A	2052	2052
	Root of squared residual error	N/A	7.955 mmol/m^3	1.651 mg/m^3
	Magnitude	N/A	−2.157 mmol/m^3	−0.2827 mg/m^3
	Abruptness	N/A	0.67	0.67
Iceland	Changepoint year	2086	2090	2073
	Root of squared residual error	171 m	9.237 mmol/m^3	1.592 mg/m^3
	Magnitude	+30.48 m	+1.239 mmol/m^3	+0.3139 mg/m^3
	Abruptness	0.91	1.10	0.71
Labrador	Changepoint year	2039	2062	2038
	Root of squared residual error	963 m	13.21 mmol/m^3	2.097 mg/m^3
	Magnitude	−269.7 m	−3.030 mmol/m^3	−0.3844 mg/m^3
	Abruptness	0.71	0.40	1.18
Irminger	Changepoint year	2039	N/A	2039
	Root of squared residual error	1,189 m	N/A	3.467 mg/m^3
	Magnitude	−154 m	N/A	−0.3008 mg/m^3
	Abruptness	0.78	N/A	1.54
Scotland	Changepoint year	2047	2048	2048
	Root of squared residual error	691 m	13.75 mmol/m^3	3.340 mg/m^3
	Magnitude	−198 m	−4.818 mmol/m^3	−0.9591 mg/m^3
	Abruptness	0.53	0.38	0.26

Note. N/A indicates no changepoint detected.

the changepoint versus the changepoint to the end of the time series. A shift from one low-noise regime to another would produce a low residual, but abrupt shifts between a noisy regime to one with low noise will have higher residuals. This metric is reported in Table 1 as the root of squared residual errors.

The magnitude of the changepoint is calculated as the difference between means for the time series up to the changepoint and the mean from the change year until 2100. The lengths of the periods either side are variable between properties and regions, and here, we use the full lengths on the assumption that the changepoint represents a formal "break" between conditions either side.

Finally, a measure of the abruptness of the change is defined based on the magnitude of change between the 10-year periods before and after the changepoint. This is listed as a fraction of the overall magnitude metric and defined as

$$\frac{mean(x_i : x_{i+10}) - mean(x_{i-10} : x_i)}{mean(x_i : x_{2100}) - mean(x_{2000} : x_i)}$$

where x is the variable to which the metric is being applied, and i is the year of the changepoint. 2000 and 2100 are the start and the end of the time series, respectively.

2.3.3. Phenology and "Collapse" of the NAB

Analysis here aims to identify a potential "collapse" of the NAB—defined here to be a factor 2 decline in surface chlorophyll—relative to present-day values. Using 5-day mean model output, the time of year in which each grid cell reached its annual maximum surface CHL concentration was extracted for each model year in the 21st century. While monthly means were considered when calculating changes in the magnitude of the bloom to
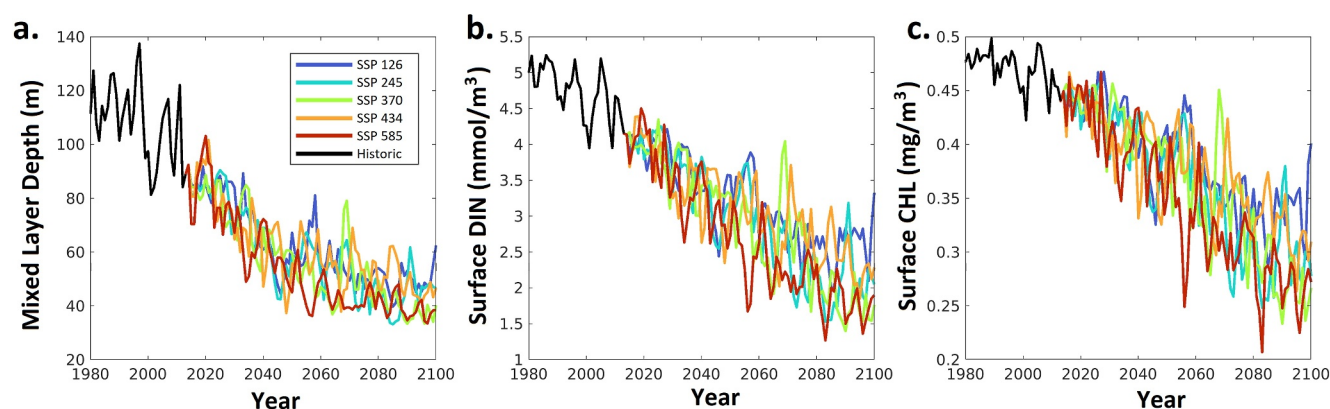
Figure 1. Time series of annual mean (a) upper mixed layer depth, (b) surface dissolved inorganic nitrogen, and (c) surface chlorophyll concentrations from UKESM1 simulated under five SSP forcing scenarios.

reduce the noise in the time series of maxima, the highest temporal frequency available is required to obtain meaningful results about the timing of the peak.

The changepoint detection algorithm (`findchangepts` MATLAB subroutine) was applied to the time series for each grid cell in the northern North Atlantic region in order to detect whether an abrupt shift in the timing of the peak of the bloom occurs and, by comparison with the changepoints detected in the magnitude of the bloom (Figures 5a–5c, 7d and 7e), to establish whether such a change coincides with the timing of abrupt changes in its magnitude.

3. Results

Experimental results are presented as follows. First, results from the low-resolution ESM (UKESM1) are shown for five boxes (per Section 2.3.1) sampling different regimes in the northern North Atlantic under five different future SSP pathways, before a comparison of the present decade and the end of the century is presented for a representative pathway (SSP370). A more detailed analysis of the UKESM results is presented in Supporting Information S1 Section S2, before moving on to the main focus on the high-resolution NEMO-MEDUSA run in Section 3.2.

In Section 3.2, upper mixed layer depth (MLD), surface dissolved inorganic nitrogen (DIN), and surface chlorophyll (CHL) are analyzed to characterize the scale and spatial patterns of changes between the present day (2020s) and the end of the century (2090s). In Section 3.3, a changepoint detection algorithm is applied to time serieses of these fields to identity abrupt changes. Finally, Section 3.4 quantifies the projected changes in the phenology of the seasonal spring bloom.

3.1. Decline of the NAB in the UKESM1

Initially, the UKESM model was analyzed over a broad zonal sector of the northern North Atlantic that encompasses the SPG and adjacent areas (56–76°N, 7–57°W). Five forcing scenarios were considered (SSP126, SSP245, SSP370, SSP434, and SSP585; see Section 2.1.1), and key properties associated with the NAB (i.e., upper mixed layer depth and surface nitrate and chlorophyll concentrations) were investigated for each. Figure 1 shows the time series of each variable over the northern North Atlantic sector.

As is clear from Figure 1a, the upper mixed layer depth (MLD) shoals in UKESM1 across this region under all scenarios, with the depth of the upper mixed layer approximately halving by the end of the century with little difference between scenarios.

Strong declines are also apparent in the modeled surface dissolved inorganic nitrogen (DIN) and chlorophyll (CHL) fields. As with the modeled change in MLD, this decline is apparent over all SSPs investigated, though there appears to be some sensitivity to forcing scenario; by the 2090s, the high-emission SSP585 features approximately 1 mol/m^3 less surface DIN and 0.1 mg/m^3 less surface chlorophyll than the low-emission SSP126 scenario.

To further explore the projected decline in the NAB, we consider SSP370 in greater detail; decadal means of peak MLD, DIN, and CHL are shown for the present decade (Figures 2a–2c) and compared with equivalents
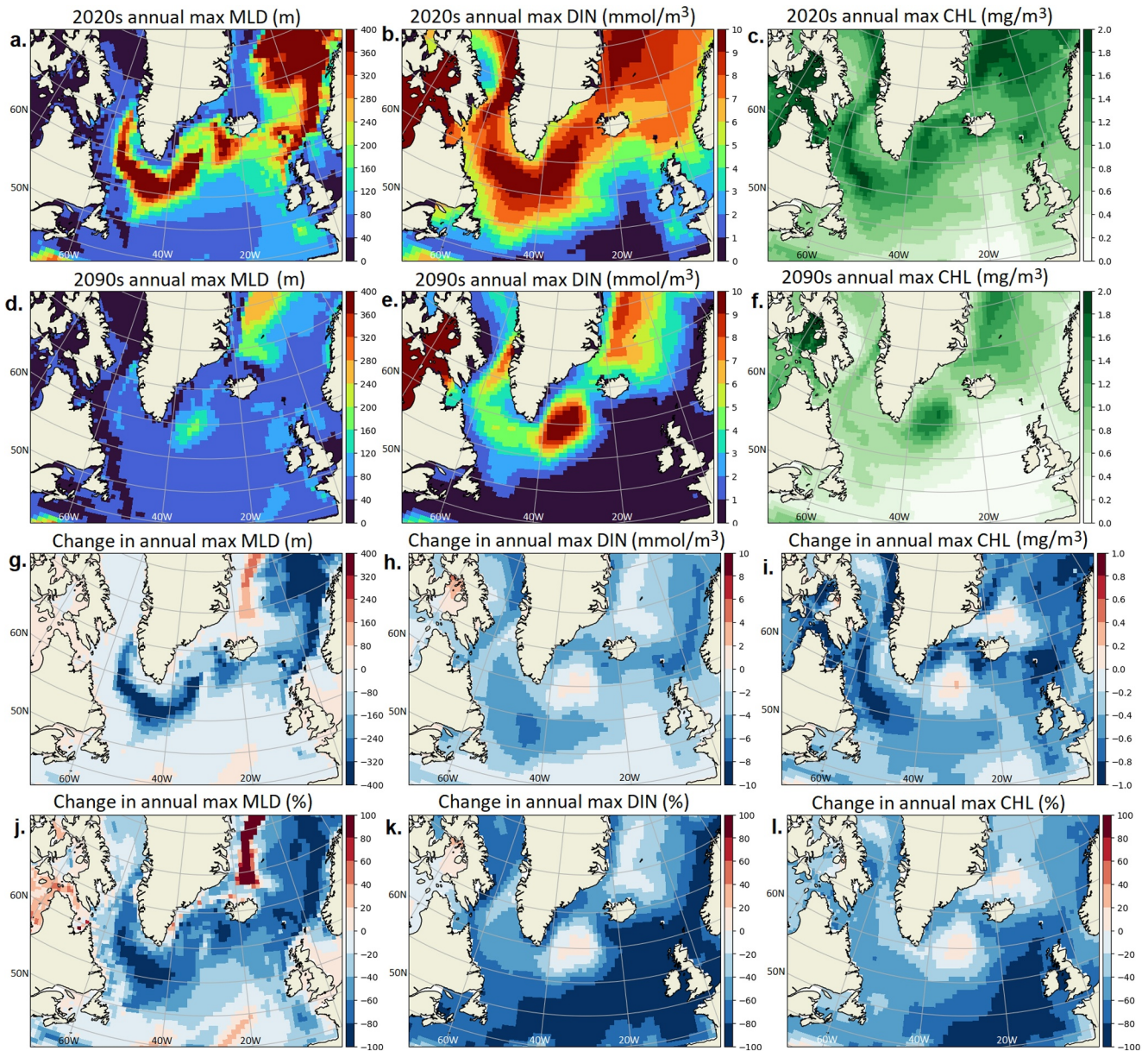
Figure 2. UKESM under SSP370: comparison of present decade (2020s; a–c) and end of the century (2090s; d–f) annual maximum mixed layer depth (left), surface dissolved inorganic nitrogen (middle), and surface chlorophyll (right). Changes between the decades are shown as both absolute (g–i) and relative (j–l) values.

for the end of the century (Figures 2d–2f). The absolute (Figures 2g–2i) and relative (Figures 2j–2l) changes are shown; all variables decline throughout the majority of the northern Atlantic, and our >50% decline in surface chlorophyll criterion for a "collapse" of the NAB is met throughout much of the northern North Atlantic.

Figures 2g and 2j indicate that one of the largest regional changes (in both absolute and relative terms) is the collapse of the upper mixed layer depth in the SPG, especially in the west of the gyre, though MLD collapse is also pronounced in the Norwegian Sea. Changepoint analysis, as described in Section 2.3.2., was applied over boxes covering the same geographic regions as described in Section 2.3.1. (and later investigated more extensively for the 1/12° resolution ocean-only run of the model). These results, shown in Supporting Information S1 (Figures S1–S4), showed abrupt changes in MLD occurring across the region during the period of 2000–2030 across all five forcing scenarios explored; see Figure S1 in Supporting Information S1. However, abrupt changes were detected in DIN and CHL. These largely coincided with each other, but not with the changes detected in MLD, with exception of the southeastern part of the domain. Given importance of resolution for the biophysical
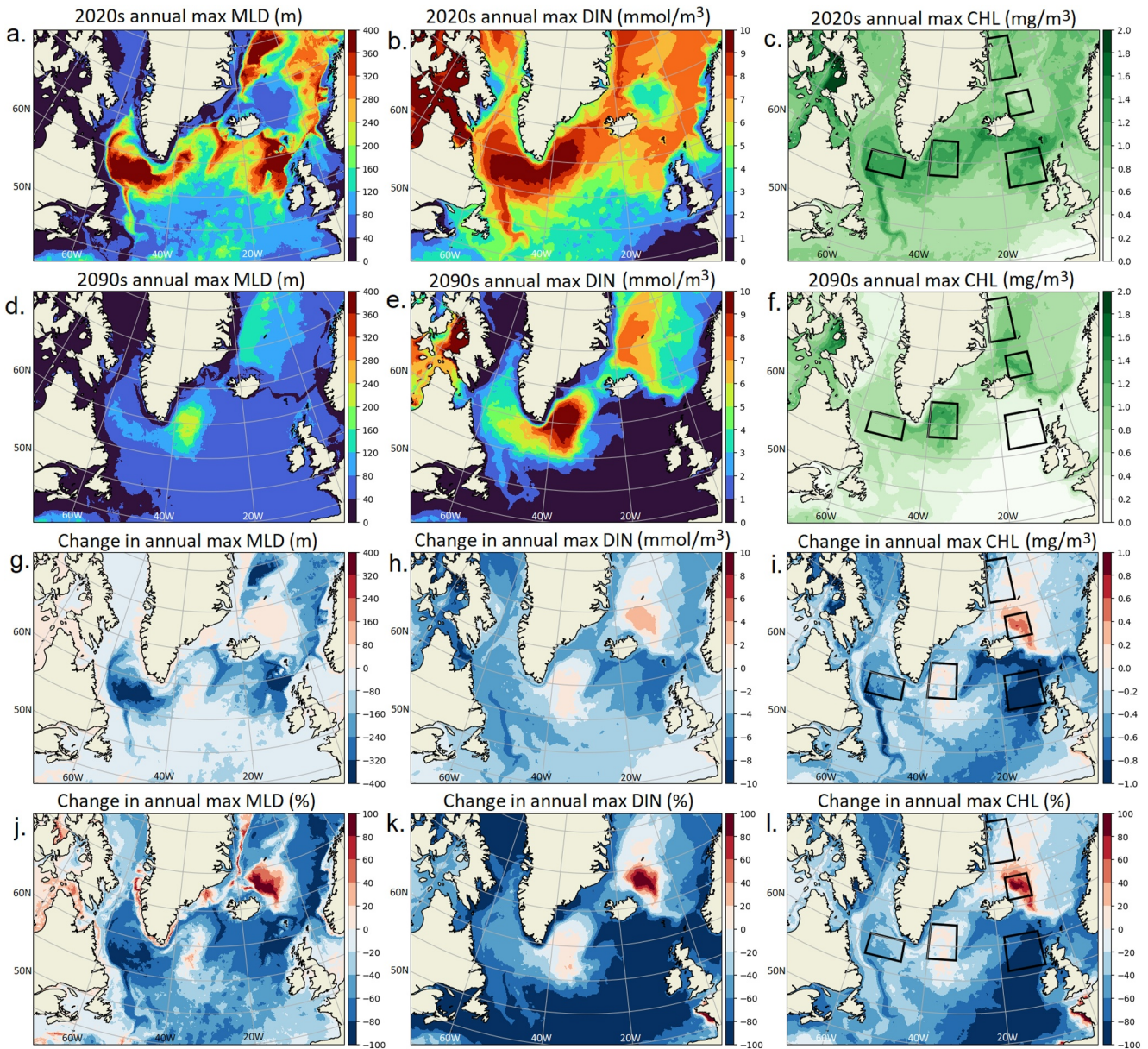
Figure 3. Comparison of the present decade (2020s; a–c) and end of the century (2090s; d–f) annual maximum mixed layer depth (left), surface dissolved inorganic nitrogen (middle), and surface chlorophyll (right) in the high-resolution ocean-only NEMO run. Changes between the decades are shown as both absolute (g–i) and relative values (j–l). The locations of the five boxes used later in the analysis are shown in the CHL panels (c, f, i and l).

interactions, this motivates a more detailed investigation of the high-resolution output from the 1/12° NEMO run, to explore whether the better representation of the ocean dynamics would present a different picture of the Chl a response to the abrupt changes in MLD.

3.2. NEMO-MEDUSA Analysis: Projected Changes in Characteristics of the NAB

In order to investigate projected changes in the NAB, modeled upper mixed layer depth, surface dissolved inorganic nitrogen, and surface chlorophyll were compared between the present day (decade 2020s; Figures 3a–3c) and the end of the century (decade 2090s; Figures 3d–3f). The decadal means of annual maxima of MLD, DIN, and CHL for these periods are shown in Figure 3, as well as the absolute (Figures 3g–3i) and relative (Figures 3j–3l) changes between decades. Each annual maximum was itself calculated from monthly means, and the annual maximum was used to highlight changes in the peak of the bloom for each variable.
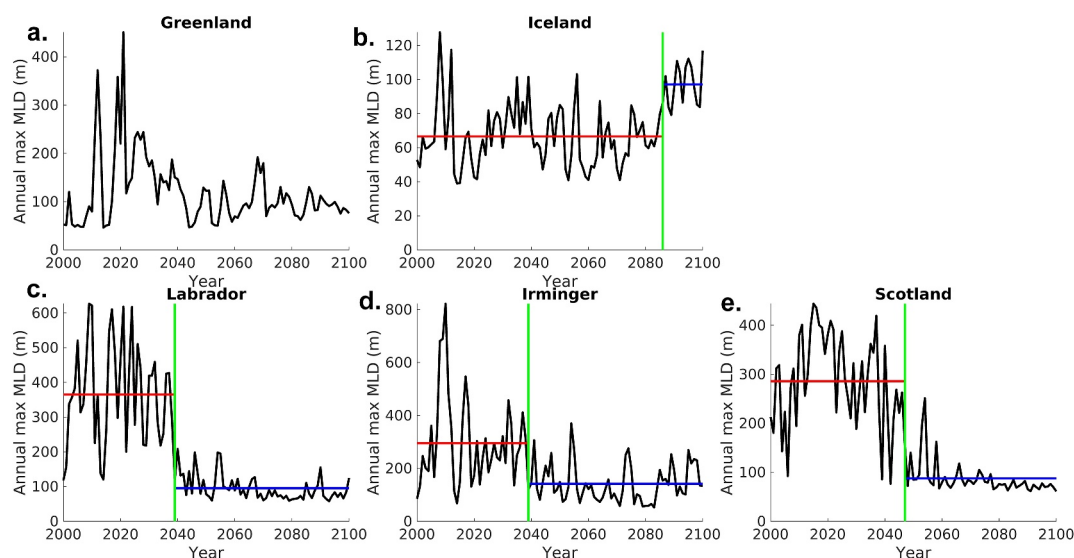
Figure 4. Time series of annual maximum MLD in each of the five boxes: (a) Greenland, (b) Iceland, (c) Labrador, (d) Iriminger, and (e) Scotland. Green lines indicated the significant changepoints, red and blue show the mean before and after changepoints, respectively (means are not shown if a changepoint is not detected). Equivalent plots for DIN and CHL are shown in Supporting Information S1 Figures S7 and S8.

From Figure 3, it is clear that pronounced reductions are projected to occur across all three bloom-relevant variables over the majority of the northern North Atlantic during the 21st century. These results are broadly consistent with the similar changes highlighted from the UKESM output shown in Figure 2. In particular, areas that are currently characterized by deep winter mixing—for instance, the SPG itself and the region northwest of Scotland—show some of the largest changes in all three variables. CHL additionally shows an even stronger response to the west of the United Kingdom, where CHL concentration drops below 0.2 mg m^{-3} (see Figure 3f). Meanwhile, the Irminger Sea south of Greenland and the Norwegian Sea northeast of Iceland are two smaller regions where mixing increases relative to the 2020s (see Figures 3g and 3j), with corresponding increases in DIN (Figures 3h and 3k) and, especially, chlorophyll (Figures 3i and 3l).

3.3. Abrupt Changes in MLD, CHL, and DIN

To further investigate these projected declines in the key variables associated with the NAB, five areas that sample different regimes within the northern North Atlantic were identified (see Section 2.3.1). Time serieses of region-averaged annual maximum MLD, DIN, and CHL were compared over each of the five boxes. Abrupt changes in each time series were determined using a changepoint analysis method (see Section 2.3.2) that detects the most statistically significant changepoint in the mean. The results of this are shown in Table 1 and graphically in Figure 4 (for MLD), with Supporting Information S1 Figures S7 and S8 showing DIN and CHL, respectively. Only the single most significant changepoint was searched for; and in some cases, no single statistically significant abrupt change was detected, and this is indicated with N/A. While the changepoint detection method does not provide an uncertainty in the timing of the changepoint, the root of squared residual error is quoted for each detected changepoint.

In order to prevent results being unduly skewed by short-term variability, fast Fourier transforms were applied to all the time series analyzed, and the dominant mode of variability was found to be multidecadal over all five boxes; this is shown in Figure S10 of the Supporting Information S1. LOESS smoothing was also applied to each time series (shown in Figure S11 of the Supporting Information S1) with negligible effect on the results. A more complete description of this analysis is presented in Section S5 of the Supporting Information S1.

The magnitude (i.e., the difference between local means before and after detected changepoints), the square root of the residual associated with each changepoint, and a metric of "abruptness" are presented in Table 1. The abruptness metric was defined as the ratio of the magnitude of change in local mean 10 years either side of the
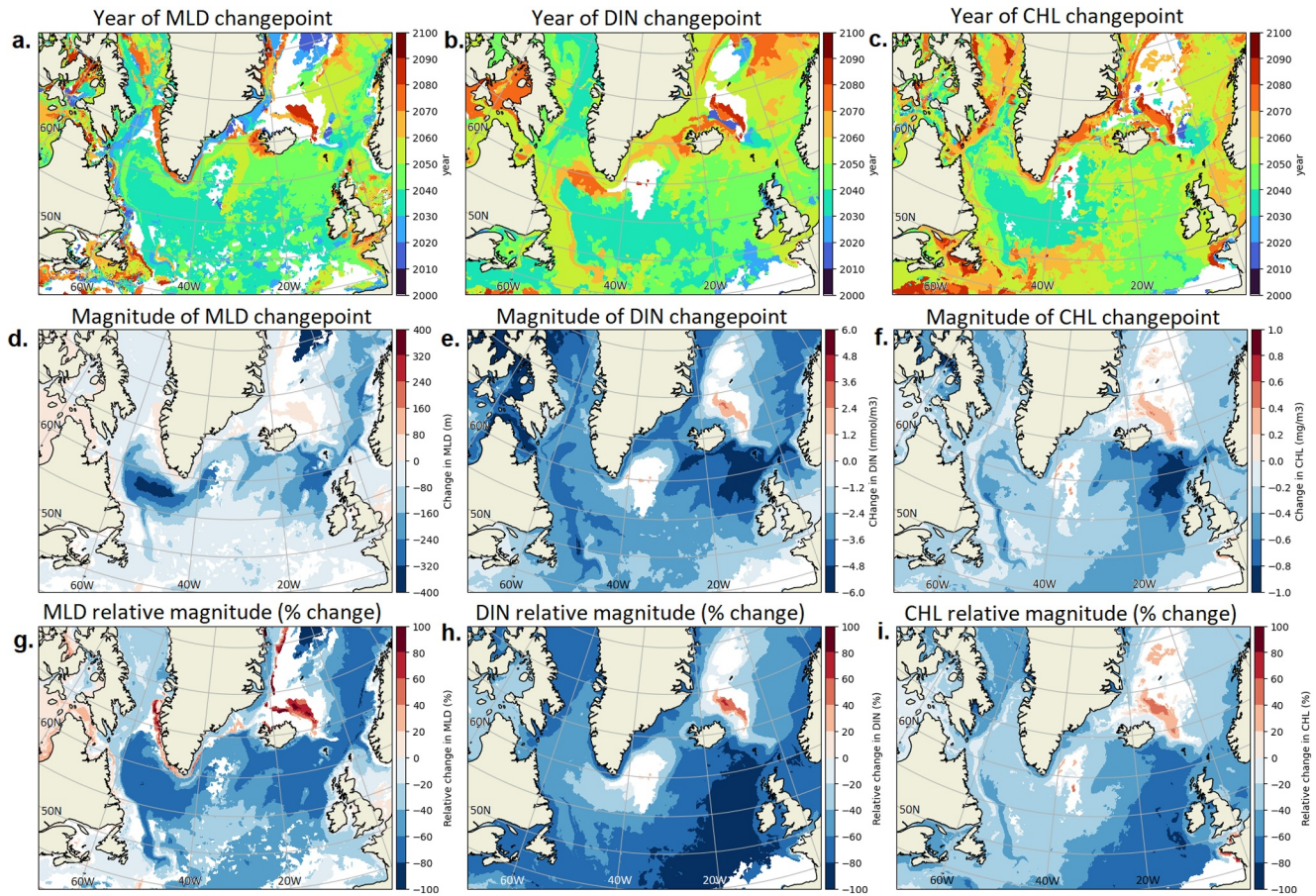
Figure 5. Year and magnitude of most significant abrupt change in annual maximum of upper MLD (left), surface DIN (middle), and surface CHL (right). Panels a–c show the timing of the abrupt change, d–f show its absolute magnitude, and g–i show the magnitude of the abrupt change relative to the prechangepoint mean.

changepoint to the overall magnitude of change for the entirety of the changepoint before/after the changepoint. For an idealized step change, the abruptness metric would be exactly equal to 1; 100% of the change would occur in a short window over the time series. (For a continuous gradual change over a century, an abruptness of 0.1 would be expected, or an abrupt change that overshoots before stabilizing can be >1.)

Statistically significant abrupt changes were identified for almost all variables and regions, with exceptions for Greenland MLD (Figure 4a) and Irminger DIN. The detected MLD changepoints for the other 4 boxes are shown graphically in Figures 4b–4e. In the case of Greenland, while a changepoint was not detected, the deep MLD values found in the first half of the 21st century do not occur in the second half (see Figure 4a). Otherwise, most of the identified changepoints fall within 1 year of each other for all variables in which a changepoint was detected. These ranged from the late 2030s in both the Labrador and Irminger regions, the late 2040s for the Scotland region (2047–2048), the early 2050s for the Greenland region, and around 2090 for the Iceland region. However, the timing of detected changepoints did not coincide closely in the Iceland Sea. This is unsurprising given the bloom in this region shows no decline by the end of the century (see Figure 3i). Overall, the coincident timing of the changes in MLD, DIN, and CHL indicates that decline in the chlorophyll bloom in these regions is driven by a reduction in available nutrients, in turn caused by a shallowing of the depth of the mixed layer during winter.

Using the same changepoint detection algorithm (cf. Methods), the same analysis was performed on a cell-by-cell grid basis across the northern North Atlantic to determine the year and magnitude of the most significant abrupt change in the same variables as previously. The results are shown in Figure 5. Grid cells in which no single significant change was detected are masked in white.

The SPG area immediately south of Greenland shows the most coherent spatial signal, with changepoints detected across all three properties uniformly during the 2030s (see Figures 5a–5c). The waters to the west and
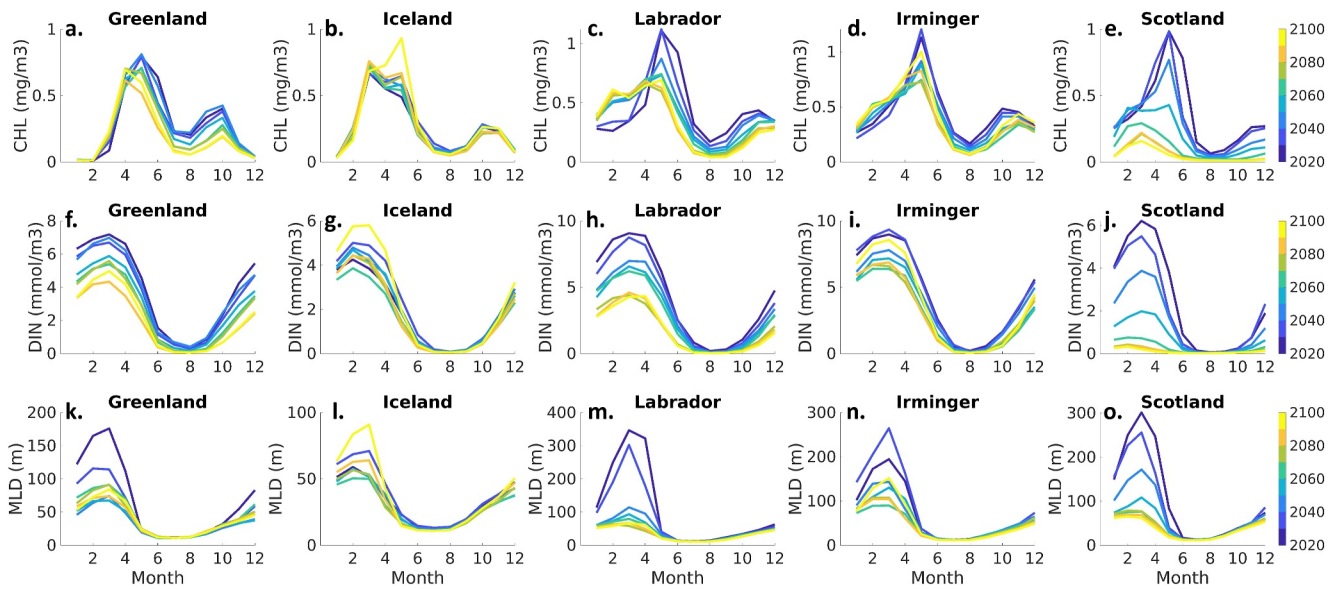
Figure 6. The changing seasonal cycle surface CHL (a–e), DIN (f–j), and MLD (k–o) of the North Atlantic bloom over the five boxes used throughout this analysis, with each decade (2020s–2090s) indicated by a different color of line.

northeast of Iceland also show broad agreement in the late-century timing of changepoints. Otherwise, the spatial relationships between the timing of MLD, DIN, and CHL changepoints can be much less clear. For instance, the eastern coastline of Greenland has changepoints detected for MLD in the 2020s (Figure 5a), for DIN in the 2050s (Figure 5b), and from the 2070s for CHL (Figure 5c).

Correlation analysis of the magnitude of changes (between 2020s and 2090s) of annual maxima for MLD, DIN, and CHL was undertaken and is presented in Section S4 of the Supporting Information S1. The magnitude of detected changepoints is shown in absolute terms in Figures 5d–5f and in relative terms in Figures 5h–5i. Statistically significant ($p \ll 0.01$) correlations were identified between MLD and DIN ($r^2 = 0.40$), DIN and CHL ($r^2 = 0.61$), and between MLD and CHL ($r^2 = 0.39$). This and associated geographic clustering are explored more thoroughly in Figure S9 of the Supporting Information S1.

Correlations were also calculated between the timings of the changepoints shown in Figures 5a–5c; these were statistically significant ($p \ll 0.01$) but weaker than the magnitude correlations; $r^2 = 0.35$ between the DIN and CHL changepoints over the northern North Atlantic region, but only $r^2 = 0.11$ and $r^2 = 0.17$ between MLD and DIN, and between MLD and CHL, respectively. In terms of the magnitude of change around the changepoints, the SPG stands out less, with a region of significant (consistently more than 60% decline) decrease occurring only in MLD (although all three properties show a stronger negative signal on the western margin of the gyre). However, all three variables (MLD, CHL, and DIN) show large negative step changes northwest of Scotland, as well as notable positive step changes northeast of Iceland—both regions where the changepoint analysis identifies common timeframes of change. Otherwise, the spatial patterns in magnitude change that are found between the different variables are much less coherent. This is likely reflective of the differing time signals from the separate changepoint analyses.

3.4. Abrupt Changes in Phenology of the NAB

Finally, we consider that, in addition to changes in the magnitude of the NAB, changes in its phenology may occur. Initially, we compare the seasonal cycles of CHL, DIN, and MLD in each of the decades between the 2020s and 2090s, over the same five illustrative boxes as used previously. This is shown in Figure 6:

Focusing on the seasonal cycles over the Greenland, Labrador, and Scotland boxes in Figure 6, we see three regions which show a pronounced decline in the NAB as well as a shift to an earlier CHL peak by the end of the century—see Figures 6a, 6c, and 6e. In particular, the Scotland box shows a dramatic collapse of peak CHL. As previously noted, the Iceland box (Figure 6b) is an exception to the overall northern North Atlantic as it shows an

increase in peak CHL by the 2090s—and a later CHL peak, while the Irminger box (Figure 6d) shows comparatively little change.

To understand potential drivers for these changes, we then consider the projected changes to the annual cycles of DIN (Figures 6f–6j) and MLD (Figures 6k–6o) and how these may affect surface CHL concentrations. Reduced surface DIN concentrations (driven by a shoaled MLD) would be expected to lead to lower CHL concentrations in seasonally nutrient limited areas, but a shallower upper mixed layer would itself allow for greater light availability in the euphotic layer, which could in turn lead to earlier phytoplankton blooming (Lacour et al., 2015).

The Greenland and Labrador boxes are both characterized by considerably shallower winter MLDs by the 2090s (Figures 6k and 6m), and in turn experience an increase in surface CHL concentrations during the first half of the year compared to the 2020s (Figures 6a and 6c). Given that DIN is >>0.5 mmol/m^3 during this period (Figures 6f and 6h, and Section S4 of the Supporting Information S1 for more discussion of DIN limitation), this is consistent with a shallower upper mixed layer allowing for an enhanced phytoplankton bloom due to increased light availability. However, the reduced DIN at the end of the century (Figures 6f and 6h) means that nutrient limitation is reached earlier in the year than at present, leading to an earlier CHL peak.

The Scotland box demonstrates a scenario where the surface DIN falls below the typical half saturation threshold year-round (Figure 6j) with a consequent collapse of surface CHL concentrations consistent with nutrient limitation.

We now move on to considering the northern North Atlantic region as a whole. Figures 7a and 7b illustrate the day of year (from 5-daily means) at which the bloom peaked averaged for the 2020s and 2090s, respectively, with 7c showing the change in timing. Finally, we repeat the analysis from Section 3.3, but applying the changepoint algorithm to the time series of the day of the year in which CHL reaches its annual maximum. The timing of detected changepoints in the timeseries of CHL peak day are shown in Figure 7d.

From Figures 7a–7c, it is apparent that throughout the vast majority of the northern North Atlantic, the decline (in some cases indicative of collapse) of magnitude of the NAB is coupled with a significant shifting of its phenology. Across large portions of the basin, the peak day of year becomes >50 days earlier. However, the shift in timing of the bloom's peak is less pronounced in two key areas: the SPG and the Iceland Sea.

While the SPG generally shows a smaller change in bloom timing, it also exhibits different behavior in its eastern and western regions. In the west, the Labrador Sea is projected to see its annual CHL peak occur approximately 30 days earlier by the 2090s. However, the east of the gyre/Irminger Sea is projected to show comparatively little change in the timing of its CHL peak between the 2020s and 2090s. Comparing Figure 7c with the 2090s CHL abundance shown in Figure 3h, it is apparent that while most of the northern North Atlantic is characterised by both a decline in surface CHL and a shift towards earlier CHL peaks, the Irminger Sea is an exception; it is projected to exhibt relatively little change in either the magnitude or timing of the CHL peak.

In the case of the Iceland Sea, comparing Figures 3i and 7c reveals that the later blooms during the 2090s in this region (by up to 50 days) coincide with the same region in which surface CHL increases by the end of the century. Overall, throughout the northern North Atlantic, a decline in the magnitude of the NAB is correlated with an earlier day of occurrence of its peak.

Finally, while no significant abrupt changes are visible in the southern portion of the region (Figure 7d), changepoints centered from around the 2040s are detected for the majority of the northern North Atlantic. Although considerable variability is found, comparing these timings with those shown in Figure 5c suggests that the detected abrupt shifts in the CHL seasonal cycle are coincident with the abrupt changes in the magnitude of the bloom.

Further analysis aimed to quantify the correlation between changes in the timing and the peak of the CHL bloom. This is presented in Figure 7e, where the colors indicate the projected changes in MLD. By linear regression, there was found to be a weaker ($r^2 = 0.26$) but statistically significant ($p << 0.01$) correlation between the changes in the timing and strength of the bloom over the northern North Atlantic.
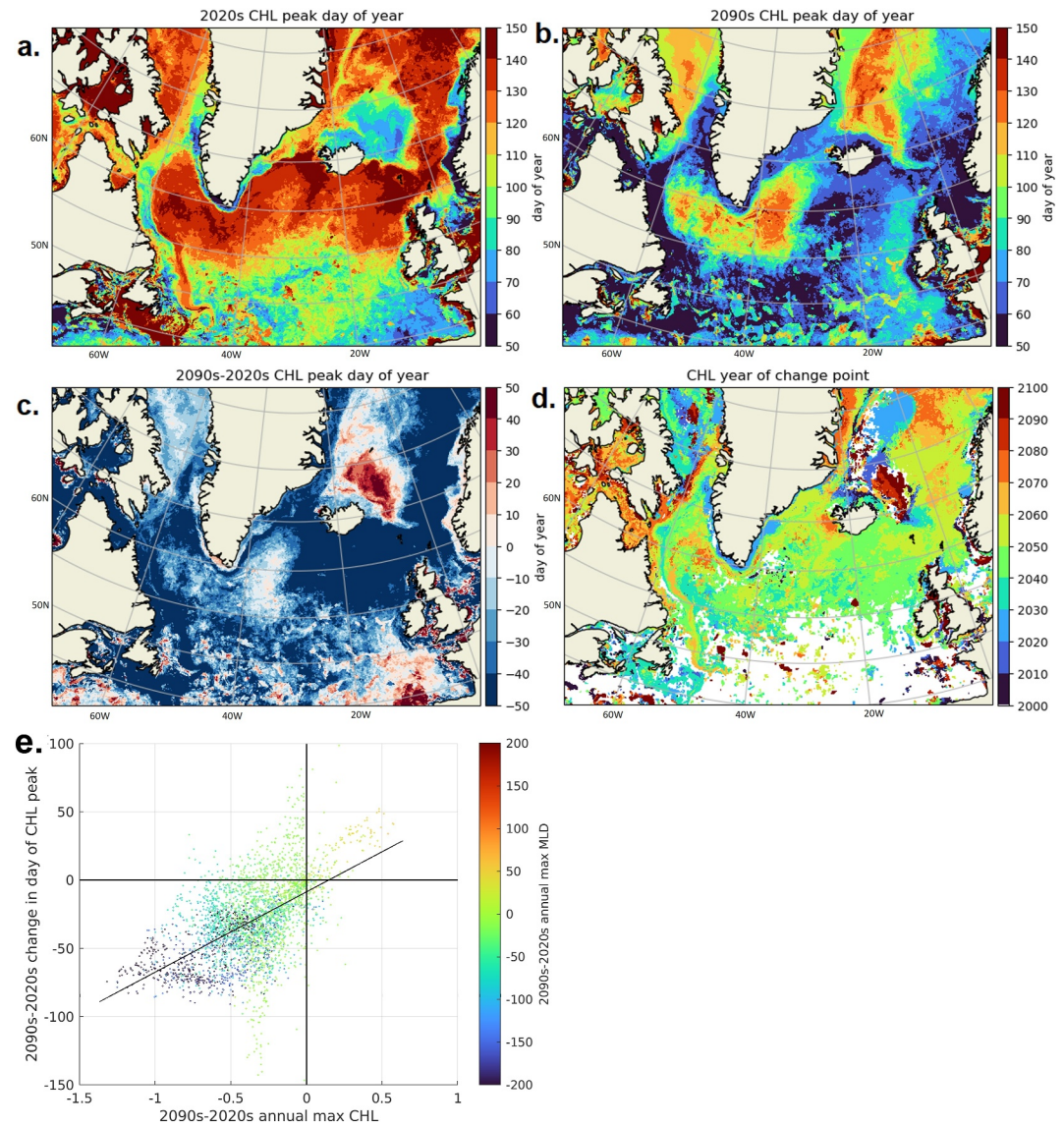
Figure 7. Change in CHL peak day. (a) Average day of annual CHL maximum in 2020s. (b) Average day of annual CHL maximum in 2090s. (c) Difference between 2020s peak day and 2090s peak day. (d) Year of CHL peak changepoint. (e) Shows the relationship between changes in the timing and strength of the CHL peak, with a statistically significant ($p <<$ 0.01) correlation ($r^2 = 0.26$) between them over the region (40–70N, 0–60W). Dots are colored by changes in MLD, averaged over 10×10 groups of cells.

4. Discussion

In the results presented here, a "collapse" (i.e., >50% decline in surface CHL) of the NAB was identified throughout much of the northern North Atlantic in both UKESM and the high-resolution NEMO ocean-only model. This is consistent with previous research in which multimodel analysis has identified the northern North Atlantic as a hotspot for the decline in net primary production, driven by the decrease in winter mixing in both CMIP5 and CMIP6 experiments (Kwiatkowski et al., 2020; Nakamura & Oka, 2019). This localized reduction in productivity is apparent even in the lower emission SSP1-2.6 scenario, where primary production over the rest of the ocean remains relatively unchanged.

The North Atlantic SPG is a regional component of the wider AMOC and is a key element of the coupled system that drives the climatic and ecological regime of the northern Atlantic Ocean and bordering landmasses. The SPG has been identified as a tipping element within the climate system, a regional climate nexus with the potential for

rapid (decadal-scale) state change in response to a combination of ocean circulation and associated atmospheric mechanisms (Armstrong McKay et al., 2022).

The repercussions of such an event would be far-reaching in the UK and Western Europe, with regime shifts in the weather patterns (Ghosh et al., 2017) impacting economic activities such as agriculture and land use, and energy demand and supply, while also changing the nature, magnitude and severity of natural hazards (Holliday et al., 2018; Swingedouw et al., 2021). In the marine environment, an SPG transition would lead to fundamental changes in patterns of ecosystem productivity such as the magnitude and timing of the NAB. This, in turn, would lead to cascading impacts on higher tropic levels, including commercial fisheries (Berx & Payne, 2017), and disrupting northern Atlantic ecosystems already "on the move" in response to other climate-driven changes (Mueter et al., 2021; Pecl et al., 2017).

Model studies predict the high-latitude North Atlantic region may experience a number of significant, causally linked changes across the 21st century. These include it becoming increasingly stratified (Kwiatkowski et al., 2020; Sgubin et al., 2017), a decrease in surface nutrient concentrations (Lavoie et al., 2017; Sein et al., 2015), a decrease in net primary production and export production (Fu et al., 2016; Kwiatkowski et al., 2020; Nakamura & Oka, 2019; Yool et al., 2015), earlier bloom initiation and/or peak (Asch, 2019; Henson et al., 2013, 2018; Sein et al., 2015; Yamaguchi et al., 2022), a reduction in diatom and coccolithophore abundance with a shift to smaller phytoplankton (Bopp et al., 2005; Fu et al., 2016; Grieve et al., 2017; Jensen et al., 2017), and a poleward and eastward migration of plankton species (Barton et al., 2016; Villarino et al., 2015). The results presented here add to that picture, with further evidence of a more stratified ocean evident from the shoaled MLDs across the North Atlantic and in particular in the SPG, widespread decline in surface nutrients (aside from in the Iceland Sea and in the east of the SPG), and consequent reduction in surface CHL by end of century.

The North Atlantic is one of only two regions (the second being the Southern Ocean) where 80% of the CMIP6 models agreed on the sign of change of the net primary production (Tagliabue et al., 2021). However, in absolute terms, the SPG is one of the three regions displaying the largest intermodel uncertainty of the primary production change (Tagliabue et al., 2021). The results presented here add detail to this story; the contrast between the Labrador Sea (which shows a decline in CHL and DIN by the end of the century) and the Irminger Sea (which shows a slight increase in both over the same timescale) demonstrates that projected changes in the SPG are not necessarily homogenous, and that the sign of the projected change can indeed be either positive or negative depending on the region in question.

Furthermore, the abrupt collapse of the phytoplankton bloom is not limited to the SPG where the high-resolution model indicates a widespread and abrupt decline in winter convection as early as the decade 2030–2040, along with an associated decline in DIN and CHL. An even more significant (in relative terms) decline in CHL occurs in the southeastern part of the domain, characterized by the subtropical inflow. In these areas west of the UK, CHL declines by an order of magnitude only a decade later (2040–2050s). Although the bloom is not as pronounced here compared to the SPG, such a dramatic change in primary producers is likely to lead to significant changes in the ecosystems and fisheries of the adjacent European shelves.

Previous research has also explored the question of how the timing of the onset and the peak of the NAB may change over the 21st century. Analysis of both CMIP5 and CMIP6 models points toward earlier onset of the phytoplankton bloom (by 0.5–1 month by 2100 under the RCP8.5 (Henson et al., 2013), in high latitudes, driven by increase in temperature and reduction in depth of winter mixing. However, Yamaguchi et al. (2022) point toward the subtle effects of decoupling between phytoplankton growth and zooplankton predation as an additional important driver of changes in the timing of the peak of the bloom. The results from our analysis suggest potential for an even greater change than the 0.5–1 month change seen in Henson's analysis. Aside from the Irminger and Iceland Seas, we see CHL peaks more than 50 days earlier across most of the northern North Atlantic. Such a pronounced shift in the timing of the bloom would likely have significant repercussions higher up the North Atlantic food web.

In the event of a collapse of the NAB, it would likely have significant consequences for the North Atlantic food web. For example, *Calanus finmarchicus* (henceforth *Calanus*), commonly known as the North Atlantic copepod or the Norwegian krill, plays a vital role in the northern North Atlantic ecosystems. Calanoid copepods, which graze on the NAB, are important secondary producers in the North Atlantic ecosystem (Melle et al., 2014) and a

crucial food source for pelagic fish larvae (Beaugrand et al., 2003; Jacobsen et al., 2022; Prokopchuk & Sentyabov, 2006) through to seabirds and whales (Defriez et al., 2016; Grieve et al., 2017; Pershing & Stamieszkin, 2020). The life-history strategies of *Calanus* have evolved to align with the timing of the phytoplankton bloom. This synchronization allows *Calanus* to take advantage of the strong seasonal pulse of their primary food source, and to store energy reserves from this in the form of lipids. During the harsh northern North Atlantic winters, *Calanus* leaves the surface mixed layer and enters diapause, a state of dormancy, allowing it to survive the winter period of very low phytoplankton availability (itself driven by dilution and light limitation). These seasonal fluctuations in the abundance and vertical position of *Calanus* in the water column have profound effects on the higher trophic levels that prey on it, including commercially important fish species and the critically endangered North Atlantic right whale (Grieve et al., 2017).

If the NAB undergoes a collapse, it is likely that there would be a considerable reduction of *Calanus* population in the SPG as a result of an abrupt change of phytoplankton phenology, and this phenological mismatch could have significant effects at higher trophic levels. The mismatch hypothesis, first described by Cushing (1969) states that predator survival depends on the match or mismatch between the timing of predator feeding and that of prey availability. Pertinent to the North Atlantic food web, Ferreira et al. (2021) explored how changes to the phenology of three different trophic levels could impact the recruitment of North Sea herring. They demonstrated that 23% of historical North Sea herring recruitment could be attributed to spatiotemporal overlap between distributions of the predator species and small copepods/phytoplankton. Asch (2019) explored the relationship between fisheries recruitment and mismatch of species life cycles under an RCP8.5 scenario and found blooms 16 days earlier at high latitudes (above 40°N). It was also found that "extreme events", where seasonal mismatches exceeded 30 days, could lead to failure of fish recruitment. Given that large areas of the North Atlantic see phenological shifts exceeding 50 days in our analysis, this strongly motivates further research into the consequences of major changes in the phenology of the North Atlantic.

Given the scale of the changes identified in our analysis, further research using an ensemble of models would be beneficial to add confidence to the conclusions presented here. We used UKESM exclusively and focussed in particular on a high-resolution ocean-only run forced by the atmosphere from UKESM under SSP370 forcing. As the high-resolution run is very computationally expensive, no other comparable run was available at the time of writing, putting a high-resolution ensemble beyond the scope of this paper. While abrupt changes have been identified, the question of whether or not they constitute irreversible tipping points remains open. Further research with ramp-up/ramp-down warming scenarios would potentially be able to answer this question.

4.1. Limitations and Future Work

Finally, there are several important caveats to note around this work. First, we are limited by only making use of a single marine physics-biogeochemistry model (NEMO-MEDUSA) in two linked configurations. In addition to limiting the range of simulated processes and future responses (cf. Kwiatkowski et al. (2020)), this also means that only a single array of model biases and limitations is considered. As noted by Yool et al. (2021) for UKESM1 but applicable here, NEMO-MEDUSA has a number of specific deficiencies, including some (most importantly nutrient biases) inherited from the model's spin-up period (Yool et al., 2020). Séférian et al. (2020) present an overview of the performance of CMIP6 models, including UKESM1, for the recent historical period, and this illustrates the variability in their performance, both geographically and between fields. The diversity in basic model performance found by Séférian et al. (2020) tends to imply that investigating the fate of the NAB between models is a productive avenue.

However, with rare exceptions, the majority of these CMIP6 ESMs are only represented by low-resolution simulations, while our study demonstrates that a high-resolution ocean-only projection shows different temporal and spatial dynamics of abrupt changes in comparison to the low-resolution UKESM under the same emission scenario. High-resolution ocean models better capture physical processes critical to marine biogeochemistry and its driving mechanisms, particularly in high latitudes where the Rossby radius is smaller (e.g., Hewitt et al., 2020). For the NAB, these include the maximum depth and seasonality of winter convection as well as advective freshwater pathways, including mesoscale eddies and boundary currents. Although 1/12-degree models resolve these key driving processes and their biogeochemical responses better than 1-degree models (e.g., Popova et al., 2016), this improved representation does not necessarily translate into improved model agreement with observed climatological fields. Such an agreement is also impacted by factors such as gaps in observationally derived initial

conditions and the effects of model drift across extended spin-up. Demonstrating improved model skill due to increased resolution requires a carefully designed set of experiments, which is beyond the scope of this manuscript.

The recent study of Hieronymus et al. (2024) provides an example of this. There, two CMIP6 models using the same future projection (SSP585) were used to investigate abrupt NAB decline. This work found similar changes to those here, with abrupt change more pronounced in the northern portion of the North Atlantic domain considered (cf. Figure 8 of Brodeau et al. (2010) vs. Figure 7d here). Interestingly, these changes were also found to occur sooner than 2050, further supporting the consistency of pre-2050 abrupt shifts in the NAB.

A second limitation here is that, for the high-resolution ocean model, computational constraints meant that only a single future projection (SSP370) was used compared with the full range sampled using the low-resolution ESM. The contrast in spatial coherence of the NAB response between the low- and high-resolution simulations suggests that a spread of future scenarios using the latter would be valuable—particularly so given the relative consistency of response across different scenarios across the range in warming of the ESM simulations. However, as noted, the computational expense of high-resolution, even for an ocean-only configuration, makes this kind of extension challenging.

A key next step in understanding the ecological consequences of the collapse of the NAB is a more detailed treatment of the mesozooplankton that form an intermediate link in the marine food web. Generally, CMIP-class models, including MEDUSA, represent this size spectrum of simpler zooplankton (if diversely; Rohr et al. (2023)). As noted earlier, this ecological group includes species such as *Calanus finmarchicus*, which, as well as being intermediary in the food chain, exhibit a structured life history that includes a seasonal period of diapause at depth. This diapause period is significant for its potential role in both match and mismatch timing (i.e., *Calanus* returning to the surface from diapause need temporal alignment with the NAB), and for the so-called lipid pump (Jónasdóttir et al., 2015), a component of the wider biological carbon pump (Sanders et al., 2014). Some models (e.g., LILICOP_1.0; Anderson et al. (2022)) formally include representation of these processes, but the level of complexity required exceeds that currently used in computationally expensive 3D models used here and across CMIP.

5. Summary and Conclusions

- The SPG is a key region for the phenomenon of the North Atlantic bloom (NAB), and potentially a vulnerable "tipping element" as climate change increases ocean stratification, altering its nutrient status and productivity.
- Here, we use simulations from a low-resolution Earth system model (UKESM1) and a high-resolution forced-ocean model (NEMO-MEDUSA) to examine the seasonal behavior of the phytoplankton across the North Atlantic.
- Analysis of UKESM1 finds the NAB "collapses"—defined as a halving of surface CHL—throughout the majority of the North Atlantic across low–high emissions scenarios, driven by a shoaling of seasonal mixing and a decline in surface nutrient availability. However, the temporal and spatial coherence of the ecosystem response to the abrupt changes in MLD was low, making prediction of changepoints difficult.
- By contrast, analysis of NEMO-MEDUSA under a single high-emissions scenario finds spatial and temporal coherence between abrupt changes in MLD and corresponding changes in DIN and CHL, occurring around decade 2030–2040 in the SPG, and 2040–2050 over the majority of the northern North Atlantic, with a particularly dramatic decline of the NAB in areas adjacent to the UK and European shelves.
- Further analysis of this abrupt change found concurrent changes in the phenology of the NAB, with blooms occurring 30 or more days earlier across large portions of the North Atlantic between 2040 and 2060.
- The combination of large changes in both the magnitude and timing of the NAB has potentially significant consequences for the basin's wider productivity and food web, with ecological mismatches leading to recruitment failures of fish stocks, significant both as a marine resource and for charismatic species such as seabirds and whales.
- Future research is required to investigate whether the abrupt regimes shifts found here in the NAB represent a true hysteresis in the North Atlantic from which recovery cannot occur on human timescales, and whether they are significant for mitigation and adaptation planning for fisheries and biodiversity.

Data Availability Statement

Data and software supporting this research are available at doi: 10.5281/zenodo.11622507 (https://zenodo.org/records/11622507) doi: 10.5281/zenodo.14538025 (https://zenodo.org/records/14538025). This includes scripts used for data processing and model data used for the creation of this manuscript; the contents of each file are described in a "readme" document included in the Zenodo repository. Observational upper mixed layer depth and surface dissolved inorganic nitrogen data from World Ocean Atlas were used in the validation section (Garcia et al., 2019; Locarnini et al., 2019), as well as chlorophyll data from the Climate Change Initiative (CCI) v5 L4 monthly 4-km resolution data set, downloaded from Copernicus Marine Environmental Monitoring Service (CMEMS, https://marine.copernicus.eu/access-data), calculated from satellite observations of ocean color as described by Gohin et al. (2002), and updated by CMEMS following the same method since.

References

Anderson, T. R., Hessen, D. O., Gentleman, W. C., Yool, A., & Mayor, D. J. (2022). Quantifying the roles of food intake and stored lipid for growth and development throughout the life cycle of a high-latitude copepod, and consequences for ocean carbon sequestration. *Frontiers in Marine Science*, 9. https://doi.org/10.3389/fmars.2022.928209

Archibald, A. T., O'Connor, F. M., Abraham, N. L., Archer-Nicholls, S., Chipperfield, M. P., Dalvi, M., et al. (2020). Description and evaluation of the UKCA stratosphere–troposphere chemistry scheme (StratTrop vn 1.0) implemented in UKESM1. *Geoscientific Model Development*, 13(3), 1223–1266. https://doi.org/10.5194/gmd-13-1223-2020

Armstrong Mckay, D. I., Staal, A., Abrams, J. F., Winkelmann, R., Sakschewski, B., Loriani, S., et al. (2022). Exceeding 1.5°C global warming could trigger multiple climate tipping points. *Science*, 377(6611), eabn7950. https://doi.org/10.1126/science.abn7950

Asch, R. G. (2019). Chapter 4 - changing seasonality of the sea: Past, present, and future. In A. M. Cisneros-Montemayor, W. W. L. Cheung, & Y. Ota (Eds.), *Predicting future oceans*. Elsevier.

Barton, A. D., Irwin, A. J., Finkel, Z. V., & Stock, C. A. (2016). Anthropogenic climate change drives shift and shuffle in North Atlantic phytoplankton communities. *Proceedings of the National Academy of Sciences*, 113(11), 2964–2969. https://doi.org/10.1073/pnas.1519080113

Beaugrand, G., Brander, K. M., Alistair Lindley, J., Souissi, S., & Reid, P. C. (2003). Plankton effect on cod recruitment in the North Sea. *Nature*, 426(6967), 661–664. https://doi.org/10.1038/nature02164

Beaulieu, C., & Killick, R. (2018). Distinguishing trends and shifts from memory in climate data. *Journal of Climate*, 31(23), 9519–9543. https://doi.org/10.1175/jcli-d-17-0863.1

Bersch, M., Yashayaev, I., & Koltermann, K. P. (2007). Recent changes of the thermohaline circulation in the subpolar North Atlantic. *Ocean Dynamics*, 57(3), 223–235. https://doi.org/10.1007/s10236-007-0104-7

Berx, B., & Payne, M. R. (2017). The sub-polar gyre index – A community data set for application in fisheries and environment research. *Earth System Science Data*, 9(1), 259–266. https://doi.org/10.5194/essd-9-259-2017

Biri, S., & Klein, B. (2019). North Atlantic sub-polar gyre climate index: A new approach. *Journal of Geophysical Research: Oceans*, 124(6), 4222–4237. https://doi.org/10.1029/2018jc014822

Bopp, L., Aumont, O., Cadule, P., Alvain, S., & Gehlen, M. (2005). Response of diatoms distribution to global warming and potential implications: A global model study. *Geophysical Research Letters*, 32(19). https://doi.org/10.1029/2005gl023653

Born, A., Stocker, T. F., Raible, C. C., & Levermann, A. (2013). Is the Atlantic subpolar gyre bistable in comprehensive coupled climate models? *Climate Dynamics*, 40(11–12), 2993–3007. https://doi.org/10.1007/s00382-012-1525-7

Bozbiyik, A., Steinacher, M., Joos, F., Stocker, T. F., & Menviel, L. (2011). Fingerprints of changes in the terrestrial carbon cycle in response to large reorganizations in ocean circulation. *Climate of the Past*, 7(1), 319–338. https://doi.org/10.5194/cp-7-319-2011

Brodeau, L., Barnier, B., Treguier, A.-M., Penduff, T., & Gulev, S. (2010). An ERA40-based atmospheric forcing for global ocean circulation models. *Ocean Modelling*, 31(3–4), 88–104. https://doi.org/10.1016/j.ocemod.2009.10.005

Clark, D. B., Mercado, L. M., Sitch, S., Jones, C. D., Gedney, N., Best, M. J., et al. (2011). The Joint UK Land Environment Simulator (JULES), model description – Part 2: Carbon fluxes and vegetation dynamics. *Geoscientific Model Development*, 4(3), 701–722. https://doi.org/10.5194/gmd-4-701-2011

Cole, H., Henson, S., Martin, A., & Yool, A. (2012). Mind the gap: The impact of missing data on the calculation of phytoplankton phenology metrics. *Journal of Geophysical Research: Oceans*, 117(C8). https://doi.org/10.1029/2012jc008249

Cushing, D. H. (1969). The regularity of the spawning season of some fishes. *ICES Journal of Marine Science*, 33(1), 81–92. https://doi.org/10.1093/icesjms/33.1.81

Daniault, N., Mercier, H., Lherminier, P., Sarafanov, A., Falina, A., Zunino, P., et al. (2016). The northern North Atlantic Ocean mean circulation in the early 21st century. *Progress in Oceanography*, 146, 142–158. https://doi.org/10.1016/j.pocean.2016.06.007

Defriez, E. J., Sheppard, L. W., Reid, P. C., & Reuman, D. C. (2016). Climate change-related regime shifts have altered spatial synchrony of plankton dynamics in the North Sea. *Global Change Biology*, 22, 2069–2080. https://doi.org/10.1111/gcb.13229

Edwards, M., & Richardson, A. J. (2004). Impact of climate change on marine pelagic phenology and trophic mismatch. *Nature*, 430(7002), 881–884. https://doi.org/10.1038/nature02808

Ferreira, A., Brotas, V., Palma, C., Borges, C., & Brito, A. C. (2021). Assessing phytoplankton bloom phenology in upwelling-influenced regions using ocean color remote sensing. *Remote Sensing*, 13(4), 675. https://doi.org/10.3390/rs13040675

Foukal, N. P., & Lozier, M. S. (2017). Assessing variability in the size and strength of the North Atlantic subpolar gyre. *Journal of Geophysical Research: Oceans*, 122(8), 6295–6308. https://doi.org/10.1002/2017jc012798

Friedland, K. D., Record, N. R., Asch, R. G., Kristiansen, T., Saba, V. S., Drinkwater, K. F., et al. (2016). Seasonal phytoplankton blooms in the North Atlantic linked to the overwintering strategies of copepods. *Elementa Science of the Anthropocene*, 4, 000099. https://doi.org/10.12952/journal.elementa.000099

Fu, W., Randerson, J. T., & Moore, J. K. (2016). Climate change impacts on net primary production (NPP) and export production (EP) regulated by increasing stratification and phytoplankton community structure in the CMIP5 models. *Biogeosciences*, 13(18), 5151–5170. https://doi.org/10.5194/bg-13-5151-2016

Garcia, H., Weathers, K., Paver, C., Smolyar, I., Boyer, T., Locarnini, R., et al. (2019). NOAA Atlas NESDIS 84 WORLD OCEAN ATLAS 2018 Volume 4: Dissolved inorganic nutrients (phosphate, nitrate and nitrate + nitrite, silicate) NOAA National Centers for environmental information WORLD OCEAN ATLAS 2018 Volume 4: Dissolved inorganic nutrients (phosphate, nitrate and nitrate+nitrite, silicate).

Ghosh, R., Müller, W. A., Baehr, J., & Bader, J. (2017). Impact of observed North Atlantic multidecadal variations to European summer climate: A linear baroclinic response to surface heating. *Climate Dynamics*, *48*(11–12), 3547–3563. https://doi.org/10.1007/s00382-016-3283-4

Gohin, F., Druon, J. N., & Lampert, L. (2002). A five channel chlorophyll concentration algorithm applied to SeaWiFS data processed by SeaDAS in coastal waters. *International Journal of Remote Sensing*, *23*(8), 1639–1661. https://doi.org/10.1080/01431160110071879

Grieve, B. D., Hare, J. A., & Saba, V. S. (2017). Projecting the effects of climate change on Calanus finmarchicus distribution within the U.S. Northeast Continental Shelf. *Scientific Reports*, *7*(1), 6264. https://doi.org/10.1038/s41598-017-06524-1

Häfker, N. S., Andreatta, G., Manzotti, A., Falciatore, A., Raible, F., & Tessmar-Raible, K. (2023). Rhythms and clocks in marine organisms. *Annual Review of Marine Science*, *15*(1), 509–538. https://doi.org/10.1146/annurev-marine-030422-113038

Häkkinen, S., & Rhines, P. B. (2004). Decline of subpolar North Atlantic circulation during the 1990s. *Science*, *304*(5670), 555–559. https://doi.org/10.1126/science.1094917

Henson, S., Cole, H., Beaulieu, C., & Yool, A. (2013). The impact of global warming on seasonality of ocean primary production. *Biogeosciences*, *10*(6), 4357–4369. https://doi.org/10.5194/bg-10-4357-2013

Henson, S. A., Cole, H. S., Hopkins, J., Martin, A. P., & Yool, A. (2018). Detection of climate change-driven trends in phytoplankton phenology. *Global Change Biology*, *24*(1), e101–e111. https://doi.org/10.1111/gcb.13886

Hewitt, H. T., Roberts, M., Mathiot, P., Biastoch, A., Blockley, E., Chassignet, E. P., et al. (2020). Resolving and parameterising the ocean mesoscale in earth system models. *Current Climate Change Reports*, *6*, 137–152. https://doi.org/10.1007/s40641-020-00164-w

Hieronymus, J., Hieronymus, M., Gröger, M., Schwinger, J., Bernadello, R., Tourigny, E., et al. (2024). Net primary production annual maxima in the North Atlantic projected to shift in the 21st century. *Biogeosciences*, *21*(9), 2189–2206. https://doi.org/10.5194/bg-21-2189-2024

Holliday, N. P., Bacon, S., Cunningham, S. A., Gary, S. F., Karstensen, J., King, B. A., et al. (2018). Subpolar North Atlantic overturning and gyre-scale circulation in the summers of 2014 and 2016. *Journal of Geophysical Research: Oceans*, *123*(7), 4538–4559. https://doi.org/10.1029/2018jc013841

Jacobsen, S., Gaard, E., & Hátún, H. (2022). Declining pre-bloom Calanus finmarchicus egg production adjacent to two major overwintering regions in the northeastern Atlantic. *Frontiers in Marine Science*, *9*. https://doi.org/10.3389/fmars.2022.822978

Jebri, F., Srokosz, M., Raitsos, D. E., Jacobs, Z. L., Sanchez-Franks, A., & Popova, E. (2024). Absence of the Great Whirl giant ocean vortex abates productivity in the Somali upwelling region. *Communications Earth & Environment*, *5*(1), 20. https://doi.org/10.1038/s43247-023-01183-9

Jensen, L. Ø., Mousing, E. A., & Richardson, K. (2017). Using species distribution modelling to predict future distributions of phytoplankton: Case study using species important for the biological pump. *Marine Ecology*, *38*(3), e12427. https://doi.org/10.1111/maec.12427

Jónasdóttir, S. H., Visser, A. W., Richardson, K., & Heath, M. R. (2015). A seasonal copepod 'lipid pump' promotes carbon sequestration in the deep North Atlantic. *bioRxiv*, 021279.

Kara, A. B., Rochford, P. A., & Hurlburt, H. E. (2000). An optimal definition for ocean mixed layer depth. *Journal of Geophysical Research*, *105*(C7), 16803–16821. https://doi.org/10.1029/2000jc900072

Khatiwala, S., Tanhua, T., Mikaloff Fletcher, S., Gerber, M., Doney, S. C., Graven, H. D., et al. (2013). Global ocean storage of anthropogenic carbon. *Biogeosciences*, *10*(4), 2169–2191. https://doi.org/10.5194/bg-10-2169-2013

Killick, R., Fearnhead, P., & Eckley, I. A. (2012). Optimal detection of changepoints with a linear computational cost. *Journal of the American Statistical Association*, *107*(500), 1590–1598. https://doi.org/10.1080/01621459.2012.737745

Kuhlbrodt, T., Jones, C. G., Sellar, A., Storkey, D., Blockley, E., Stringer, M., et al. (2018). The low-resolution version of HadGEM3 GC3.1: Development and evaluation for global climate. *Journal of Advances in Modeling Earth Systems*, *10*(11), 2865–2888. https://doi.org/10.1029/2018ms001370

Kwiatkowski, L., Torres, O., Bopp, L., Aumont, O., Chamberlain, M., Christian, J. R., et al. (2020). Twenty-first century ocean warming, acidification, deoxygenation, and upper-ocean nutrient and primary production decline from CMIP6 model projections. *Biogeosciences*, *17*(13), 3439–3470. https://doi.org/10.5194/bg-17-3439-2020

Lacour, L., Claustre, H., Prieur, L., & D'Ortenzio, F. (2015). Phytoplankton biomass cycles in the North Atlantic subpolar gyre: A similar mechanism for two different blooms in the Labrador Sea. *Geophysical Research Letters*, *42*(13), 5403–5410. https://doi.org/10.1002/2015GL064540

Lavoie, D., Lambert, N., & Gilbert, D. (2017). Projections of future trends in biogeochemical conditions in the northwest Atlantic using CMIP5 Earth system models. *Atmosphere-Ocean*, *57*(1), 18–40. https://doi.org/10.1080/07055900.2017.1401973

Lenton, T. M., Held, H., Kriegler, E., Hall, J. W., Lucht, W., Rahmstorf, S., & Schellnhuber, H. J. (2008). Tipping elements in the Earth's climate system. *Proceedings of the National Academy of Sciences*, *105*(6), 1786–1793. https://doi.org/10.1073/pnas.0705414105

Locarnini, R., Mishonov, A., Baranova, O., Boyer, T., Zweng, M., Garcia, H., et al. (2019). World Ocean Atlas 2018, Volume 1: Temperature.

Madec, G., & Imbard, M. (1996). A global ocean mesh to overcome the North Pole singularity. *Climate Dynamics*, *12*(6), 381–388. https://doi.org/10.1007/BF00211684

Martin, P., Lampitt, R. S., Jane Perry, M., Sanders, R., Lee, C., & D'Asaro, E. (2011). Export and mesopelagic particle flux during a North Atlantic spring diatom bloom. *Deep Sea Research Part I: Oceanographic Research Papers*, *58*(4), 338–349. https://doi.org/10.1016/j.dsr.2011.01.006

McQueen, K., & Marshall, C. T. (2017). Shifts in spawning phenology of cod linked to rising sea temperatures. *ICES Journal of Marine Science*, *74*(6), 1561–1573. https://doi.org/10.1093/icesjms/fsx025

Melle, W., Runge, J., Head, E., Plourde, S., Castellani, C., Licandro, P., et al. (2014). The North Atlantic Ocean as habitat for Calanus finmarchicus: Environmental factors and life history traits. *Progress in Oceanography*, *129*, 244–284. https://doi.org/10.1016/j.pocean.2014.04.026

Mueter, F. J., Planque, B., Hunt, G. L., Jr., Alabia, I. D., Hirawake, T., Eisner, L., et al. (2021). Possible future scenarios in the gateways to the Arctic for Subarctic and Arctic marine systems: II. Prey resources, food webs, fish, and fisheries. *ICES Journal of Marine Science*, *78*(9), 3017–3045. https://doi.org/10.1093/icesjms/fsab122

Mulcahy, J. P., Jones, C. G., Rumbold, S. T., Kuhlbrodt, T., Dittus, A. J., Blockley, E. W., et al. (2023). UKESM1.1: Development and evaluation of an updated configuration of the UK Earth system model. *Geoscientific Model Development*, *16*(6), 1569–1600. https://doi.org/10.5194/gmd-16-1569-2023

Mulcahy, J. P., Jones, C., Sellar, A., Johnson, B., Boutle, I. A., Jones, A., et al. (2018). Improved aerosol processes and effective radiative forcing in HadGEM3 and UKESM1. *Journal of Advances in Modeling Earth Systems*, *10*(11), 2786–2805. https://doi.org/10.1029/2018ms001464

Nakamura, Y., & Oka, A. (2019). CMIP5 model analysis of future changes in ocean net primary production focusing on differences among individual oceans and models. *Journal of Oceanography*, *75*(5), 441–462. https://doi.org/10.1007/s10872-019-00513-w

O'Neill, B. C., Tebaldi, C., Van Vuuren, D. P., Eyring, V., Friedlingstein, P., Hurtt, G., et al. (2016). The scenario model intercomparison project (ScenarioMIP) for CMIP6. *Geoscientific Model Development*, *9*, 3461–3482. https://doi.org/10.5194/gmd-9-3461-2016

Payton, L., Noirot, C., Last, K. S., Grigor, J., Hüppe, L., Conway, D. V. P., et al. (2022). Annual transcriptome of a key zooplankton species, the copepod Calanus finmarchicus. *Ecology and Evolution*, *12*(2), e8605. https://doi.org/10.1002/ece3.8605

Pecl, G. T., Araújo, M. B., Bell, J. D., Blanchard, J., Bonebrake, T. C., Chen, I.-C., et al. (2017). Biodiversity redistribution under climate change: Impacts on ecosystems and human well-being. *Science*, *355*(6332), eaai9214. https://doi.org/10.1126/science.aai9214

Pérez, F., Mercier, H., Vázquez-Rodríguez, M. E. T. A. L., Lherminier, P., Velo, A., Pardo, P. C., et al. (2013). Atlantic Ocean CO2 uptake reduced by weakening of the meridional overturning circulation. *Nature Geoscience*, *6*(2), 146–152. https://doi.org/10.1038/ngeo168

Pérez, F. F., Vázquez-Rodríguez, M., Mercier, H., Velo, A., Lherminier, P., & Ríos, A. F. (2010). Trends of anthropogenic CO2 storage in North Atlantic water masses. *Biogeosciences*, *7*(5), 1789–1807. https://doi.org/10.5194/bg-7-1789-2010

Pershing, A., & Stamieszkin, K. (2020). The North Atlantic Ecosystem, from Plankton to Whales. *Annual Review of Marine Science*. *12*. https://doi.org/10.1146/annurev-marine-010419-010752

Popova, E., Yool, A., Byfield, V., Cochrane, K., Coward, A. C., Salim, S. S., et al. (2016). From global to regional and back again: Common climate stressors of marine ecosystems relevant for adaptation across five ocean warming hotspots. *Global Change Biology*, *22*(6), 2038–2053. https://doi.org/10.1111/gcb.13247

Prokopchuk, I., & Sentyabov, E. (2006). Diets of herring, mackerel, and blue whiting in the Norwegian Sea in relation to Calanus finmarchicus distribution and temperature conditions. *ICES Journal of Marine Science*, *63*(1), 117–127. https://doi.org/10.1016/j.icesjms.2005.08.005

Reverdin, G., Friedman, A. R., Chafik, L., Holliday, N. P., Szekely, T., Valdimarsson, H., & Yashayaev, I. (2019). North Atlantic extratropical and subpolar gyre variability during the last 120 years: A gridded dataset of surface temperature, salinity, and density. Part 1: Dataset validation and RMS variability. *Ocean Dynamics*, *69*(3), 385–403. https://doi.org/10.1007/s10236-018-1240-y

Rhein, M., Kieke, D., Hüttl-Kabus, S., Roessler, A., Mertens, C., Meissner, R., et al. (2011). Deep water formation, the subpolar gyre, and the meridional overturning circulation in the subpolar North Atlantic. *Deep Sea Research Part II: Topical Studies in Oceanography*, *58*(17–18), 1819–1832. https://doi.org/10.1016/j.dsr2.2010.10.061

Ritchie, J., & Dowlatabadi, H. (2017). Why do climate change scenarios return to coal? *Energy*, *140*, 1276–1291. https://doi.org/10.1016/j.energy.2017.08.083

Rodionov, S. N. (2004). A sequential algorithm for testing climate regime shifts. *Geophysical Research Letters*, *31*(9). https://doi.org/10.1029/2004gl019448

Rohr, T., Richardson, A. J., Lenton, A., Chamberlain, M. A., & Shadwick, E. H. (2023). Zooplankton grazing is the largest source of uncertainty for marine carbon cycling in CMIP6 models. *Communications Earth and Environment*, *4*(1), 212. https://doi.org/10.1038/s43247-023-00871-w

Ruggieri, E. (2013). A Bayesian approach to detecting change points in climatic records. *International Journal of Climatology*, *33*(2), 520–528. https://doi.org/10.1002/joc.3447

Sanchez-Franks, A., Holliday, N. P., Evans, D. G., Fried, N., Tooth, O., Chafik, L., et al. (2024). The Irminger Gyre as a key driver of the subpolar North Atlantic overturning. *Geophysical Research Letters*, *51*(8), e2024GL108457. https://doi.org/10.1029/2024gl108457

Sanders, R., Henson, S. A., Koski, M., De la Rocha, C. L., Painter, S. C., Poulton, A. J., et al. (2014). The biological carbon pump in the North Atlantic. *Progress in Oceanography*, *129*, 200–218. https://doi.org/10.1016/j.pocean.2014.05.005

Séférian, R., Berthet, S., Yool, A., Palmiéri, J., Bopp, L., Tagliabue, A., et al. (2020). Tracking improvement in simulated marine biogeochemistry between CMIP5 and CMIP6. *Current Climate Change Reports*, *6*(3), 95–119. https://doi.org/10.1007/s40641-020-00160-0

Sein, D. V., Mikolajewicz, U., Gröger, M., Fast, I., Cabos, W., Pinto, J. G., et al. (2015). Regionally coupled atmosphere-ocean-sea ice-marine biogeochemistry model ROM: 1. Description and validation. *Journal of Advances in Modeling Earth Systems*, *7*, 268–304. https://doi.org/10.1002/2014ms000357

Sellar, A. A., Jones, C. G., Mulcahy, J. P., Tang, Y., Yool, A., Wiltshire, A., et al. (2019). UKESM1: Description and evaluation of the U.K. Earth system model. *Journal of Advances in Modeling Earth Systems*, *11*(12), 4513–4558. https://doi.org/10.1029/2019MS001739

Sgubin, G., Swingedouw, D., Drijfhout, S., Mary, Y., & Bennabi, A. (2017). Abrupt cooling over the North Atlantic in modern climate models. *Nature Communications*, *8*(1), 14375. https://doi.org/10.1038/ncomms14375

Sparks, T. H., & Menzel, A. (2002). Observed changes in seasons: An overview. *International Journal of Climatology*, *22*(14), 1715–1725. https://doi.org/10.1002/joc.821

Storkey, D., Blaker, A. T., Mathiot, P., Megann, A., Aksenov, Y., Blockley, E. W., et al. (2018). UK global ocean GO6 and GO7: A traceable hierarchy of model resolutions. *Geoscientific Model Development*, *11*(8), 3187–3213. https://doi.org/10.5194/gmd-11-3187-2018

Swingedouw, D., Bily, A., Esquerdo, C., Borchert, L. F., Sgubin, G., Mignot, J., & Menary, M. (2021). On the risk of abrupt changes in the North Atlantic subpolar gyre in CMIP6 models. *Annals of the New York Academy of Sciences*, *1504*(1), 187–201. https://doi.org/10.1111/nyas.14659

Tagliabue, A., Kwiatkowski, L., Bopp, L., Butenschön, M., Cheung, W., Lengaigne, M., & Vialard, J. (2021). Persistent uncertainties in ocean net primary production climate change projections at regional scales raise challenges for assessing impacts on ecosystem services. *Frontiers in Climate*, *3*. https://doi.org/10.3389/fclim.2021.738224

Treguier, A. M., De Boyer Montégut, C., Bozec, A., Chassignet, E. P., Fox-Kemper, B., Mcc Hogg, A., et al. (2023). The mixed-layer depth in the Ocean model intercomparison project (OMIP): Impact of resolving mesoscale eddies. *Geoscientific Model Development*, *16*(13), 3849–3872. https://doi.org/10.5194/gmd-16-3849-2023

Vancoppenolle, M. R. C., Blockley, E., Aksenov, Y., Feltham, D., Fichefet, T., Garric, G., et al. (2023). SI3, the NEMO sea ice engine (4.2release_doc1.0).

Villarino, E., Chust, G., Licandro, P., Butenschön, M., Ibaibarriaga, L., Larrañaga, A., & Irigoien, X. (2015). Modelling the future biogeography of North Atlantic zooplankton communities in response to climate change. *Marine Ecology Progress Series*, *531*, 121–142. https://doi.org/10.3354/meps11299

Walker, G. (2006). The tipping point of the iceberg. *Nature*, *441*(7095), 802–805. https://doi.org/10.1038/441802a

Williams, K. D., Copsey, D., Blockley, E. W., Bodas-Salcedo, A., Calvert, D., Comer, R., et al. (2018). The met office global coupled model 3.0 and 3.1 (GC3.0 and GC3.1) configurations. *Journal of Advances in Modeling Earth Systems*, *10*(2), 357–380. https://doi.org/10.1002/2017ms001115

Wiltshire, A. J., Burke, E. J., Chadburn, S. E., Jones, C. D., Cox, P. M., Davies-Barnard, T., et al. (2021). JULES-CN: A coupled terrestrial carbon–nitrogen scheme (JULES vn5.1). *Geoscientific Model Development*, *14*(4), 2161–2186. https://doi.org/10.5194/gmd-14-2161-2021

Yamaguchi, R., Rodgers, K. B., Timmermann, A., Stein, K., Schlunegger, S., Bianchi, D., et al. (2022). Trophic level decoupling drives future changes in phytoplankton bloom phenology. *Nature Climate Change*, *12*(5), 469–476. https://doi.org/10.1038/s41558-022-01353-1

Yashayaev, I., & Loder, J. W. (2017). Further intensification of deep convection in the Labrador Sea in 2016. *Geophysical Research Letters*, *44*(3), 1429–1438. https://doi.org/10.1002/2016gl071668

Yool, A., Palmiéri, J., Jones, C. G., De Mora, L., Kuhlbrodt, T., Popova, E. E., et al. (2021). Evaluating the physical and biogeochemical state of the global ocean component of UKESM1 in CMIP6 historical simulations. *Geoscientific Model Development*, *14*(6), 3437–3472. https://doi.org/10.5194/gmd-14-3437-2021

Yool, A., Palmiéri, J., Jones, C. G., Sellar, A. A., De Mora, L., Kuhlbrodt, T., et al. (2020). Spin-up of UK Earth system model 1 (UKESM1) for CMIP6. *Journal of Advances in Modeling Earth Systems*, *12*(8), e2019MS001933. https://doi.org/10.1029/2019ms001933

Yool, A., Popova, E. E., & Anderson, T. R. (2013). MEDUSA-2.0: An intermediate complexity biogeochemical model of the marine carbon cycle for climate change and ocean acidification studies. *Geoscientific Model Development*, *6*(5), 1767–1811. https://doi.org/10.5194/gmd-6-1767-2013

Yool, A., Popova, E. E., & Coward, A. C. (2015). Future change in ocean productivity: Is the Arctic the new Atlantic? *Journal of Geophysical Research: Oceans*, *120*(12), 7771–7790. https://doi.org/10.1002/2015jc011167